




## Article

# A Process for Carbon Dioxide Capture Using Schiff Bases Containing a Trimethoprim Unit

Anaheed A. Yaseen <sup>1</sup>, Emaad T. B. Al-Tikrity <sup>1</sup>, Gamal A. El-Hiti <sup>2,\*</sup> , Dina S. Ahmed <sup>3</sup>, Mohammed A. Baashen <sup>4</sup> , Mohammed H. Al-Mashhadani <sup>5</sup> and Emad Yousif <sup>5</sup> 

<sup>1</sup> Department of Chemistry, College of Science, Tikrit University, Tikrit 34001, Iraq; ch@sc.nahrainuniv.edu.iq (A.A.Y.); emaad1954@tu.edu.iq (E.T.B.A.-T.)

<sup>2</sup> Cornea Research Chair, Department of Optometry, College of Applied Medical Sciences, King Saud University, P.O. Box 10219, Riyadh 11433, Saudi Arabia

<sup>3</sup> Department of Medical Instrumentation Engineering, Al-Mansour University College, Baghdad 64021, Iraq; dina.saadi@muc.edu.iq

<sup>4</sup> Department of Chemistry, College of Science and Humanities, Shaqra University, Dawadmi 11911, Saudi Arabia; mbaashen@su.edu.sa

<sup>5</sup> Department of Chemistry, College of Science, Al-Nahrain University, Baghdad 64021, Iraq; mohammed.mashhadani@ced.nahrainuniv.edu.iq (M.H.A.-M.); emad.yousif@ced.nahrainuniv.edu.iq (E.Y.)

\* Correspondence: gelhiti@ksu.edu.sa; Tel.: +966-11469-3778; Fax: +966-11469-3536

**Abstract:** Environmental problems associated with the growing levels of carbon dioxide in the atmosphere due to the burning of fossil fuels to satisfy the high demand for energy are a pressing concern. Therefore, the design of new materials for carbon dioxide storage has received increasing research attention. In this work, we report the synthesis of three new Schiff bases containing a trimethoprim unit and the investigation of their application as adsorbents for carbon dioxide capture. The reaction of trimethoprim and aromatic aldehydes in acid medium gave the corresponding Schiff bases in 83%–87% yields. The Schiff bases exhibited surface areas ranging from 4.15 to 20.33 m<sup>2</sup>/g, pore volumes of 0.0036–0.0086 cm<sup>3</sup>/g, and average pore diameters of 6.64–1.4 nm. An excellent carbon dioxide uptake (27–46 wt%) was achieved at high temperature and pressure (313 K and 40 bar, respectively) using the Schiff bases. The 3-hydroxyphenyl-substituted Schiff base, which exhibited a *meta*-arrangement, provided the highest carbon dioxide uptake (46 wt%) due to its higher surface area, pore volume, and pore diameter compared with the other two derivatives with a *para*-arrangement.

**Keywords:** Schiff bases; carbon storage media; synthesis; trimethoprim unit; surface area; adsorption; *meta*-substituted arrangement



**Citation:** Yaseen, A.A.; Al-Tikrity, E.T.B.; El-Hiti, G.A.; Ahmed, D.S.; Baashen, M.A.; Al-Mashhadani, M.H.; Yousif, E. A Process for Carbon Dioxide Capture Using Schiff Bases Containing a Trimethoprim Unit. *Processes* **2021**, *9*, 707. <https://doi.org/10.3390/pr9040707>

Academic Editor: Carmen Bacariza

Received: 4 April 2021

Accepted: 15 April 2021

Published: 16 April 2021

**Publisher's Note:** MDPI stays neutral with regard to jurisdictional claims in published maps and institutional affiliations.



**Copyright:** © 2021 by the authors. Licensee MDPI, Basel, Switzerland. This article is an open access article distributed under the terms and conditions of the Creative Commons Attribution (CC BY) license (<https://creativecommons.org/licenses/by/4.0/>).

## 1. Introduction

The consumption of fuel has increased significantly over the years because of the continuous growth of energy-demanding human activities. The burning of fuels leads to high levels of carbon dioxide (CO<sub>2</sub>) in the atmosphere [1], with the contribution of fossil fuels to the emission of CO<sub>2</sub> representing approximately 60% [2]. The main contributors to the increased CO<sub>2</sub> emission into the atmosphere are pharmaceutical and agrochemical plants. Global warming and climate change are associated with high levels of CO<sub>2</sub> emission [3,4]. In particular, these environmental changes have led to an increase in the level of seas and oceans, which can cause flooding, acidic rains, and the collapse of the global economy [5,6]. Unfortunately, the rapid reduction of the level of CO<sub>2</sub> in the atmosphere is hindered by the large-scale consumption of fuels, which is difficult to reduce in the short run. Therefore, to overcome the environmental problems associated with global warming, research has been devoted to the development of strategies for reducing the level of CO<sub>2</sub>, such as the design of new materials for efficient CO<sub>2</sub> uptake [7–10].

Various processes have been established for the capture and storage of CO<sub>2</sub>, resulting in the reduction of its concentration in the atmosphere [11–16]. The capture technique

requires the separation of CO<sub>2</sub> from other gases at a high pressure followed by its adsorption [17]. The design of new materials for CO<sub>2</sub> capture and storage has attracted increasing research attention [18–20]. The most common commercial absorbents for CO<sub>2</sub> are bases such as potassium carbonate, aqueous ammonia, and ethanolamine [21–23]. The process using ammonia, in which ammonium carbonate is produced, is simple. However, the use of ammonia or ethanolamine is not convenient because of their volatility, high energy demand, and high operational cost [24]. Therefore, alternative adsorbents with specific characteristics such as nonvolatility, recyclability, reusability, high adsorption capacity, and long life are still needed [25–27]. In addition, the application of such materials should be cost- and energy-effective.

Metal-containing adsorbents (e.g., metal oxides) have ionic and basic properties and can thus be used to capture CO<sub>2</sub>. The exothermic process of CO<sub>2</sub> adsorption using metal oxides leads to the formation of metal carbonates [28,29]. However, metal oxides exhibit limited CO<sub>2</sub> selectivity and adsorption capacity. Other materials with high chemical and thermal stability and large surface area and pore volume have been used for CO<sub>2</sub> capture, including zeolites [30] and activated carbons [31], among others [32]. However, the use of these materials for CO<sub>2</sub> capture is accompanied by various disadvantages related to their poor selectivity or hydrophilic properties, which render them unsuitable to be used with flue gases. The CO<sub>2</sub> adsorption capacity of carbon-containing materials can be enhanced using a base. For example, the combination of polyacrylonitrile and potassium hydroxide was proved to be a good medium for CO<sub>2</sub> capture under mild conditions (25 °C and 1 bar) [33]. In addition, the CO<sub>2</sub> uptake capacity of a resorcinol–formaldehyde matrix was high when potassium carbonate was used [34]. In this context, metal–organic frameworks (MOFs) can act as CO<sub>2</sub> adsorbents because of their high surface area, low adsorption heat [35], and formation of strong interactions with CO<sub>2</sub> through hydrogen bonding [36]. Similarly, porous organic polymers (POPs) are suitable for CO<sub>2</sub> capture because they are low-density, stable materials with tunable structures. The skeleton of POPs can accommodate various polar groups, organic units, and heteroatoms that can increase their adsorption capacity toward CO<sub>2</sub> [37] by facilitating its coordination. However, the use of metals in the production of POPs causes environmental problems that require attention [38]. Therefore, the development of new materials for CO<sub>2</sub> adsorption is still an active area of research. Several other useful strategies have been used to reduce the level of CO<sub>2</sub>. For example, the CO<sub>2</sub> mitigation through the direct photoreduction by sunlight and the catalytic hydrogenation to hydrocarbons can be efficient [39]. Some progress has been made using such an approach.

In the quest for new adsorbents for CO<sub>2</sub> capture, we turned our attention to heterocyclic compounds containing a 2,4-diaminopyrimidine moiety, because they are useful as biologically active compounds [40]. In particular, trimethoprim, which is used as an antibiotic to treat various infections [41], contains two different aromatic rings and is characterized by high nitrogen (19.3%) and oxygen (16.5%) contents. Considering that these characteristics could be beneficial for CO<sub>2</sub> adsorption, we attempted the synthesis of new trimethoprim Schiff bases and investigated their application in CO<sub>2</sub> capture. Recently, a range of materials has been designed, synthesized, and used to capture CO<sub>2</sub> [42–49].

## 2. Materials and Methods

### 2.1. Materials

Chemicals were obtained from Merck (Schnelldorf, Germany).

### 2.2. Instrumentations

Fourier transform infrared (FTIR) spectra were recorded on an FTIR 8300 Shimadzu spectrophotometer (Tokyo, Japan) using KBr pellets. The carbon, hydrogen, and nitrogen contents of the Schiff bases were determined using a Vario EL III elemental analyzer (Elementar Americas Inc., Ronkonkoma, NY, USA). Scanning electron microscopy (SEM; 25 kV) images were captured using a KYKY-EM3200 microscope (Ontario, CA, USA).

Nitrogen ( $N_2$ ) adsorption–desorption isotherms (77 K) were performed on a Quantachrome analyzer (Quantachrome Instruments, Boynton Beach, FL, USA). Before the measurements, the samples were dried (120 °C) under a flow of dry  $N_2$  (2 h) using a vacuum oven (Cascade TEK, Cornelius, OR, USA). The Brunauer–Emmett–Teller (BET) equation was used to calculate the specific surface area (relative pressure ( $P/P_0$ ) = 0.98). The pore size distribution was determined using the Barrett–Joyner–Halenda (BJH) method.

### 2.3. Adsorption Experiment

The  $CO_2$  uptake (313 K and 40 bar) experiments were performed on an H-sorb 2600 high-pressure volumetric adsorption analyzer (Gold APP Instrument Corporation, Beijing, China) equipped with two degassing and analyzing ports that worked simultaneously. Optimization of the pressure condition required repeating the  $CO_2$  uptake experiment more than 10 times. To the measuring tube containing a sample of the Schiff base, a known quantity of  $CO_2$  was injected until equilibrium between the adsorbed gas and the Schiff base was reached. The final equilibrium pressure was recorded automatically using. The adsorbed quantity of  $CO_2$  was calculated from the generated data.

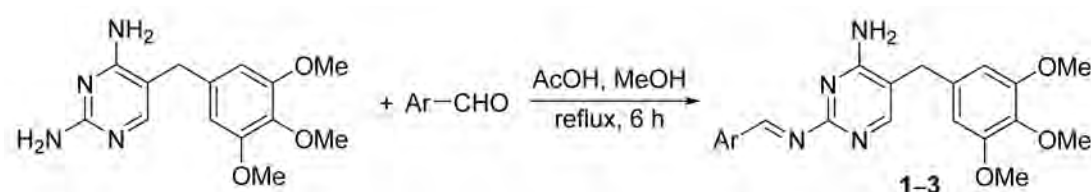
### 2.4. Synthesis of Schiff Bases 1–3

A mixture of trimethoprim (2.9 g, 10 mmol) and 3-hydroxybenzaldehyde, 4-anisaldehyde, or 4-(dimethylamino)benzaldehyde (10 mmol) in boiling methanol (MeOH; 25 mL) containing glacial acetic acid (AcOH; 0.5 mL) was refluxed while being continuously stirred for 6 h. The solid obtained on cooling to room temperature was collected through filtration, washed with MeOH (10 mL), and dried to give the corresponding Schiff base **1**, **2**, or **3** (their FTIR spectrum in Supplementary Materials Figures S1–S3).

## 3. Results and Discussion

### 3.1. Synthesis of Schiff Bases 1–3

The condensation of equimolar equivalents of trimethoprim and an aromatic aldehyde (3-hydroxybenzaldehyde, 4-anisaldehyde, or 4-(dimethylamino)benzaldehyde) in boiling MeOH in an acidic medium for 6 h gave the corresponding Schiff bases **1–3** (Scheme 1) in 83%–87% yields (Table 1). The reaction accommodates different substituents (hydroxy, methoxy, and dimethylamino) at different positions (*meta* and *para*) of the aryl ring.



Scheme 1. Synthesis of Schiff bases 1–3.

Table 1. Characteristic physical properties of Schiff bases 1–3.

Schiff Base	Color	Ar	Yield (%)	Melting Point (°C)	Calculated (Found; %)		
					C	H	N
<b>1</b>	Yellow	3-HOC <sub>6</sub> H <sub>4</sub>	85	179–181	63.95 (64.09)	5.62 (5.69)	14.20 (14.28)
<b>2</b>	White	4-MeOC <sub>6</sub> H <sub>4</sub>	83	188–190	64.69 (64.72)	5.92 (5.95)	13.72 (13.77)
<b>3</b>	Pearl yellow	4-Me <sub>2</sub> NC <sub>6</sub> H <sub>4</sub>	87	76–79	65.54 (65.55)	6.46 (6.48)	16.62 (16.68)

The FTIR spectra of **1–3** showed characteristic absorption bands in the 1655–1657  $cm^{-1}$  region due to the vibrations of the CH=N bonds (Table 2). In addition, absorption bands corresponding to the vibrations of the  $NH_2$ , CH, C=N, and C=C groups in the aromatic systems were observed in the regions of 3446–3447, 3109–3127, 1589–1591, and 1506–1543  $cm^{-1}$ , re-

spectively. Moreover, the FTIR spectrum of **1** (Supplementary Materials Figure S1) showed a broad absorption band at  $3317\text{ cm}^{-1}$  attributable to the vibration of the OH group.

**Table 2.** Fourier transform infrared ( $\nu$ ,  $\text{cm}^{-1}$ ) absorption bands of Schiff bases **1–3**.

Schiff Base	C=C	C=N (Ar)	C=N	CH (Ar)	OH	NH <sub>2</sub>
1	1543	1589	1657	3109	3317	3447
2	1506	1591	1655	3121	—	3446
3	1506	1589	1657	3127	—	3447

### 3.2. SEM of **1–3**

SEM was used to analyze the surface morphology of **1–3**. This technique can detect the presence of impurities and provides information about the homogeneity of the sample and the size and shape of the particles [50]. The SEM images ( $10\ \mu\text{m}$ ) of **1–3** (Figures 1–3) indicated the presence of a relatively uniform and amorphous surface with particles of different shapes and sizes. The surface morphology of the Schiff bases was similar in terms of pore size and shape. The pore dimension was found to be in the range of  $33.6\text{--}41.7\text{ nm}$  for **1**,  $29.5\text{--}39.0\text{ nm}$  for **2**, and  $24.9\text{--}53.7\text{ nm}$  for **3**, which are comparable with those of telmisartan tin complexes ( $20\text{--}50\text{ nm}$ ) [43] and fusidate metal complexes ( $29\text{--}50\text{ nm}$ ) [45] and smaller than those of carvedilol metal complexes ( $51\text{--}394\text{ nm}$ ) [42], melamine Schiff bases ( $20\text{--}392\text{ nm}$ ) [46], polysilicates ( $35\text{--}208\text{ nm}$ ) [47], and polyphosphates ( $28\text{--}981\text{ nm}$ ) [48,49].

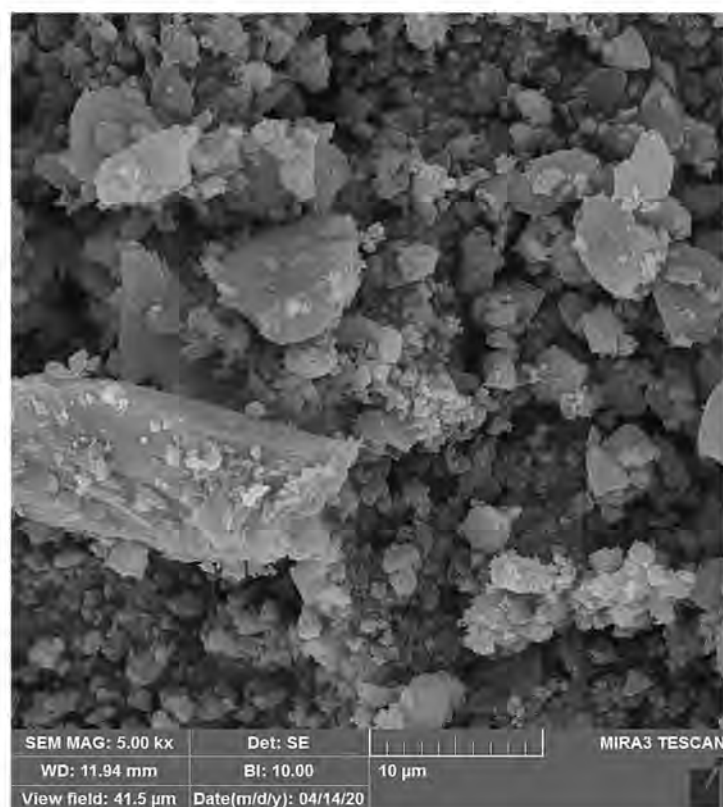


**Figure 1.** The SEM for the surface of Schiff base **1**.

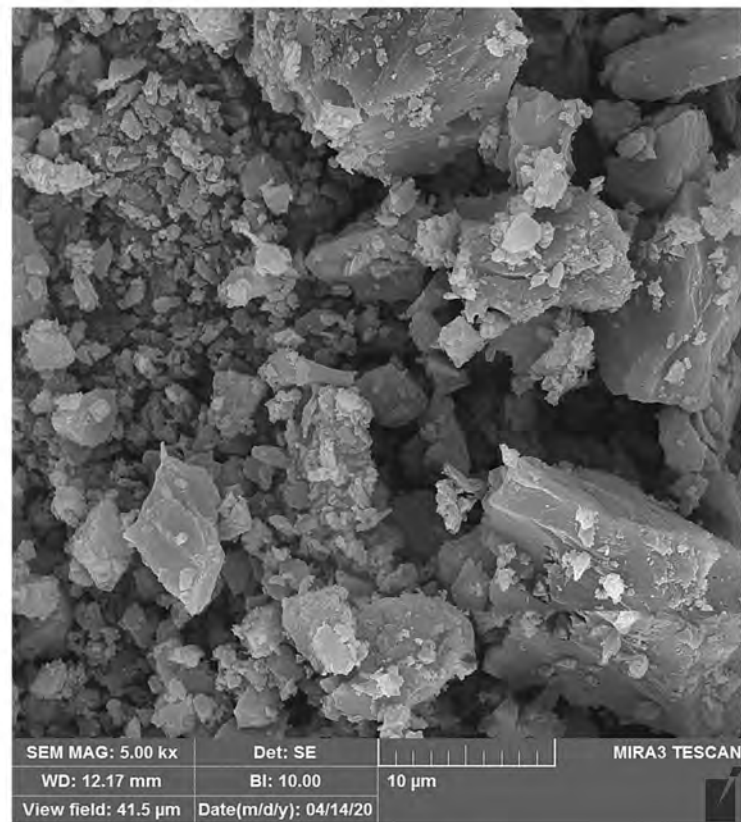


Figure 2. The SEM for the surface of Schiff base 2.

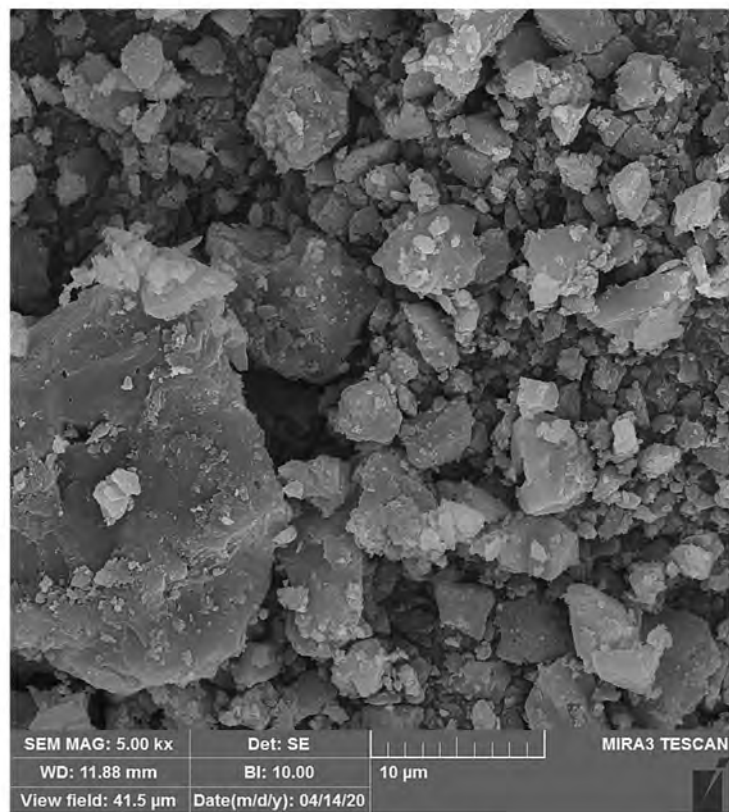


Figure 3. The SEM for the surface of Schiff base 3.

### 3.3. N<sub>2</sub> Isotherms, Surface Area and Pore Size Distribution of 1–3

The quantity of gas uptake, measured using a gravimetric tool, controls the shape of corresponding physisorption isotherms [51] and provides information about the strength of the interactions between the gas and the adsorbent. The N<sub>2</sub> isotherms for both adsorption and desorption processes using Schiff bases 1, 2, and 3 are presented in Figures 4–6, respectively. Type III isotherms were observed in all cases, indicating the absence of monolayers and the presence of relatively weak interactions between the gas and adsorbents. The isotherms started at the origin, suggesting that the heat of adsorption was similar to the heat of condensation. The adsorption of gas on the surface of the Schiff bases was favorable, leading to a sharp increase in the adsorption as the pressure increased [52].

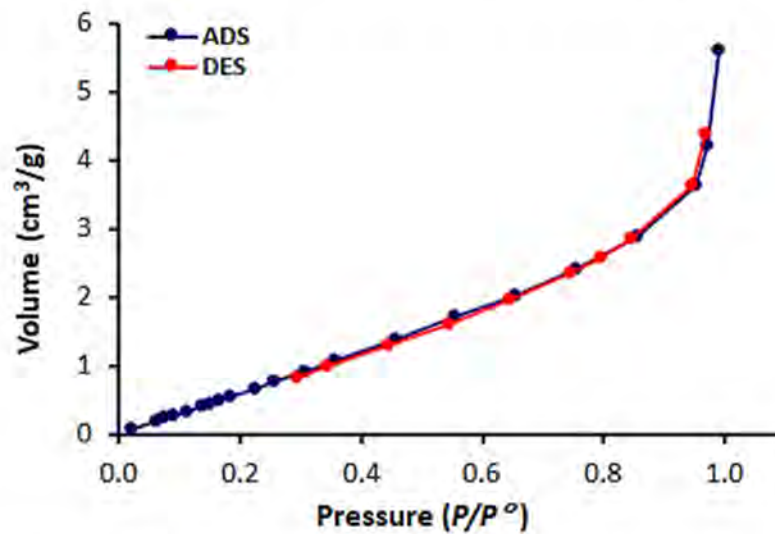


Figure 4. N<sub>2</sub> adsorption (ADS) and desorption (DES) isotherms of Schiff base 1.

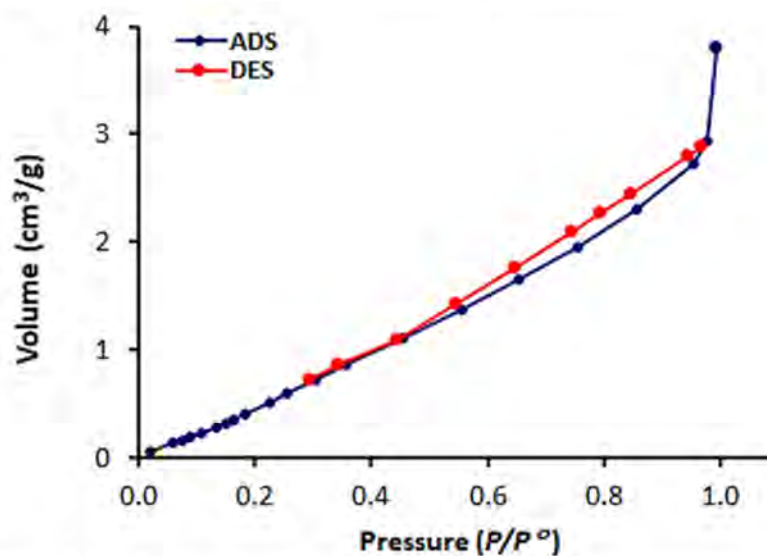


Figure 5. N<sub>2</sub> adsorption (ADS) and desorption (DES) isotherms of Schiff base 2.

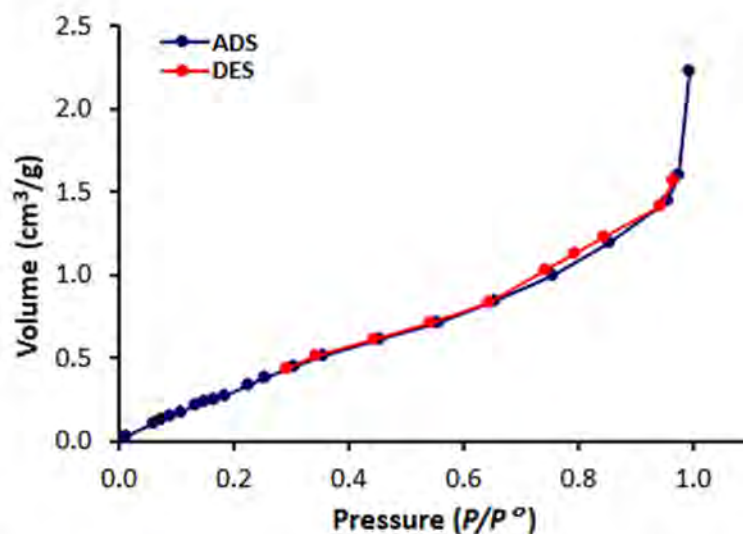


Figure 6. N<sub>2</sub> adsorption (ADS) and desorption (DES) isotherms of Schiff base 3.

The porosity of 1–3, which provides information about their interactions with the adsorbed gas, was determined at 77 K from the N<sub>2</sub> adsorption–desorption isotherms using the BJH method [53], and the specific surface area was calculated using the BET method [54]. The pore size distributions of 1–3 are illustrated in Figure 7, and the porosity values are summarized in Table 3. As can be extracted from these results, the Schiff bases had mesoporous structures with average pore diameters ranging from 6.6 to 11.4 nm which is consistent with many of our previous work. Schiff base 1 had the largest pore volume (0.0086 cm<sup>3</sup>/g) and diameter (11.4 nm). Materials with pores diameter of 10 to 15 nm have been proven to be optimal for adsorption [55]. The specific surface areas of 1–3 were low, with Schiff base 1 with a *meta* arrangement (Figure 8) exhibiting the highest surface area (20.3 m<sup>2</sup>/g). The surface areas of trimethoprim Schiff bases (4.2–20.3 m<sup>2</sup>/g) were relatively larger than those of carvedilol metal complexes (6.1–9.0 m<sup>2</sup>/g) [42], melamine Schiff bases (5.2–11.6 m<sup>2</sup>/g) [46], and polysilicates (8.2–18.0 m<sup>2</sup>/g) [47], albeit smaller than those of telmisartan tin complexes (32.4–130.4 m<sup>2</sup>/g) [43], valsartan metal complexes (16.0–22.8 m<sup>2</sup>/g) [44], fusidate metal complexes (31.2–46.9 m<sup>2</sup>/g) [45], and polyphosphates (24.8–213.5 m<sup>2</sup>/g) [48,49].

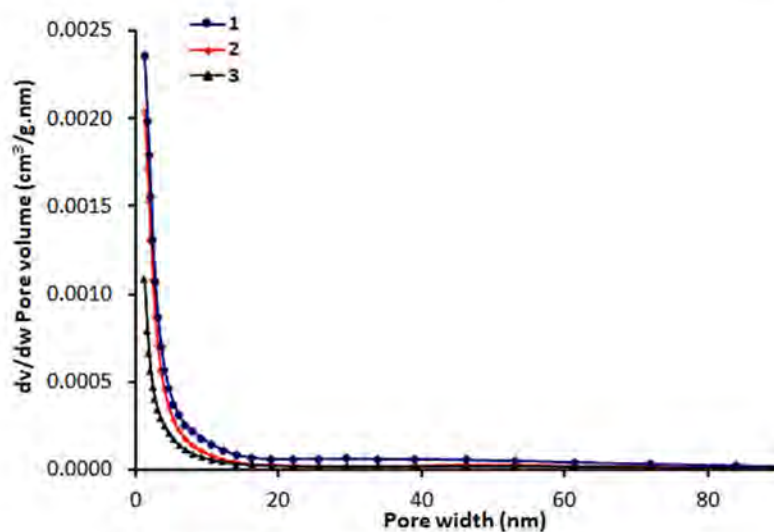


Figure 7. Pore size distributions of Schiff bases 1–3.

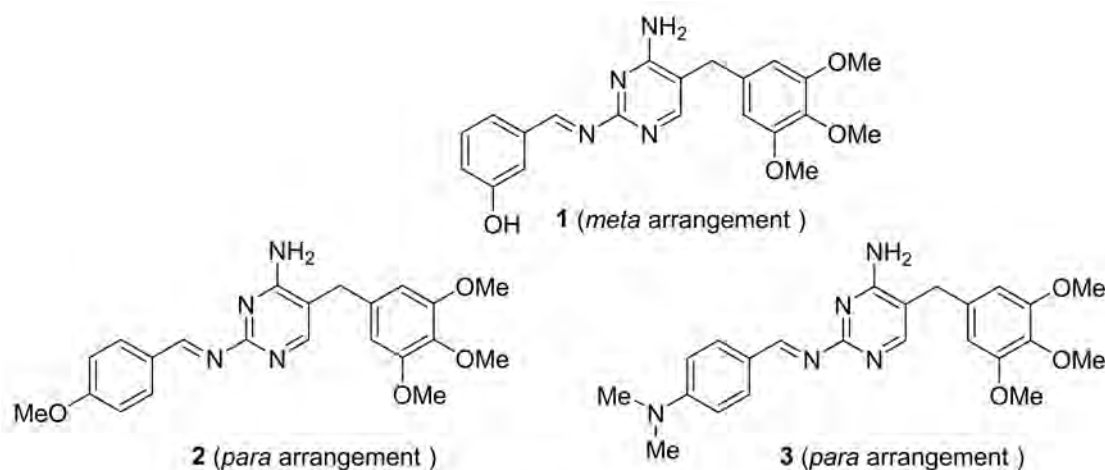


Figure 8. *meta*-arrangement in 1 and *para*-arrangement in 2 and 3.

Table 3. Porosity of Schiff bases 1–3.

Schiff Base	Specific Surface Area (m <sup>2</sup> /g)	Pore Volume (cm <sup>3</sup> /g)	Average Pore Diameter (nm)
1	20.3	0.0086	11.4
2	19.8	0.0067	8.3
3	4.2	0.0036	6.6

### 3.4. CO<sub>2</sub> Uptake of 1–3

Various factors influence the adsorption of CO<sub>2</sub> over an adsorbent, including pressure, temperature, pore volume and size, and surface area of the adsorbent materials. In addition, the magnitude of the interaction between CO<sub>2</sub> and the adsorbent is highly important [56,57]. A series of experiments were performed to optimize the pressure condition (1–40 bar). The CO<sub>2</sub> adsorption isotherms of 1–3 at 313 K and 40 bar are shown in Figure 9, and the CO<sub>2</sub> uptake results are listed in Table 4. Excellent CO<sub>2</sub> uptake (up to 46 wt%) was achieved over the present Schiff bases. This high CO<sub>2</sub> adsorption capacity can be attributed to the appropriate pore size distribution (shape, volume, and diameter) and the strong van der Waals interaction between adsorbents 1–3 and CO<sub>2</sub>. Moreover, the adsorption of gas could be further enhanced by the possible formation of hydrogen bonding between CO<sub>2</sub> and the –HC=N–, OH, and NH<sub>2</sub> moieties of the Schiff bases. The polar nature of the heteroatoms (N and O) contained in the Schiff bases could contribute to the interaction between CO<sub>2</sub> and the adsorbents. In addition, the strong Lewis base nature of 1–3 could be conducive to the CO<sub>2</sub> capture. In fact, porous materials containing heteroatoms such as N, O, Si, and P have been used as CO<sub>2</sub> adsorbents [47–49].

Table 4. CO<sub>2</sub> uptake capacity of Schiff bases 1–3<sup>a</sup>.

Schiff Base	CO <sub>2</sub> Uptake (cm <sup>3</sup> /g)	CO <sub>2</sub> Uptake (mmol/g)	CO <sub>2</sub> Uptake (wt%)
1	230.2	10.3	46
2	214.6	9.6	43
3	133.7	6.0	27

<sup>a</sup> Measurements were performed at 313 K and 40 bar.



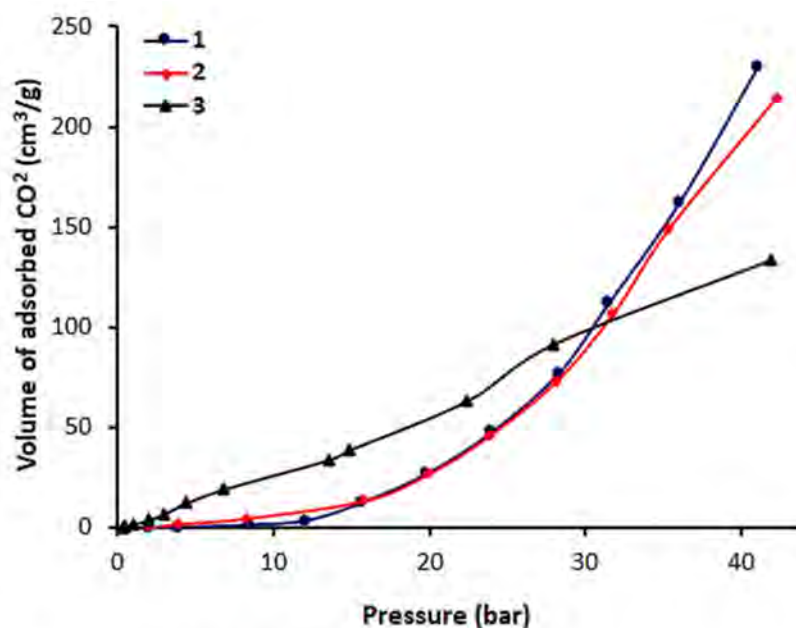


Figure 9. CO<sub>2</sub> adsorption isotherms of Schiff bases 1–3.

Schiff base **1**, with a *meta*-arrangement, exhibited the highest CO<sub>2</sub> uptake (46 wt%), followed by **2** (43 wt%) and **3** (27 wt%), which have a *para*-arrangement (Figure 8). Both **1** and **2** have a higher surface area (20.3 and 20.8 m<sup>2</sup>/g, respectively) than that of **3** (20.8 m<sup>2</sup>/g). In addition, **1** and **2** have larger pore volume and diameter than those of **3**. The present results indicate that not only the surface area of the adsorbents but also their porosity affected the adsorption capacity, being the effect of the latter particularly important. Indeed, although the surface areas of **1–3** were low, their CO<sub>2</sub> uptake was remarkable. Clearly, the high CO<sub>2</sub> adsorption capacity over Schiff base **1** can be due to a combination of various factors including pore volume and diameter and a strong interaction with CO<sub>2</sub>.

The CO<sub>2</sub> capture over **1–3** was much better than over other adsorbents under similar conditions (high pressures and temperatures) [42–49]. For instance, CO<sub>2</sub> adsorption capacity over metal complexes containing a carvedilol moiety was very limited (2.1–3.5 wt%) [42]. The efficiency of nickel (3.5 wt%) and copper (3.3 wt%) complexes was higher than that of a cobalt complex (2.1 wt%). Organotin complexes bearing a telmisartan unit afforded CO<sub>2</sub> uptake of 7.1 wt% [43], and that over valsartan metal complexes was as low as 6.8 wt% [44]. The CO<sub>2</sub> uptake over a manganese fusidate complex, which has a relatively high surface area, was 7.2 wt% [45]. The CO<sub>2</sub> uptake over copper (6.7 wt%) and zinc fusidate (6.3 wt%) complexes was lower than that over a manganese-containing adsorbent. Better CO<sub>2</sub> uptake (10.0 wt%) was observed over Schiff bases containing a melamine unit, which have very small surface areas [46]. CO<sub>2</sub> uptake of 6.0 wt% was achieved over polysilicates with a *meta*-arrangement [47], and highly aromatic polyphosphates achieved much better CO<sub>2</sub> uptake (14.0 wt%) [48]. By contrast, other polyphosphates with a high surface area led to low CO<sub>2</sub> uptake (6.0 wt%) [49]. Other materials with high surface areas, such as nanocarbons, afforded reasonable CO<sub>2</sub> uptake under mild pressure and temperature conditions [31–33].

#### 4. Conclusions

An efficient and simple process is developed for the synthesis of three new Schiff bases containing a trimethoprim moiety. The Schiff bases, which have mesoporous structures with a small surface area, act as strong Lewis bases and promote electrostatic interactions with CO<sub>2</sub>, exhibiting a high CO<sub>2</sub> adsorption capacity. The 3-hydroxyphenyl-substituted derivative with a *meta*-arrangement has the highest surface area and pore size distribution and serves as an efficient CO<sub>2</sub> storage material compared with its counterparts exhibiting a *para*-arrangement. The results presented herein demonstrate that the newly synthesized

Schiff bases are more efficient as adsorbents for CO<sub>2</sub> capture than other reported porous materials under similar conditions.

**Supplementary Materials:** The following are available online at <https://www.mdpi.com/article/10.3390/pr9040707/s1>, Figure S1: FTIR spectrum of **1**, Figure S2: FTIR spectrum of **2**, and Figure S3: FTIR spectrum of **3**.

**Author Contributions:** Conceptualization and experimental design: E.T.B.A.-T., G.A.E.-H., D.S.A., M.A.B., M.H.A.-M., and E.Y.; experimental work and data analysis: A.A.Y.; writing—original draft preparation: G.A.E.-H., D.S.A., and E.Y.; and writing—review and editing: G.A.E.-H., D.S.A., and E.Y. All authors have read and agreed to the published version of the manuscript.

**Funding:** The authors are grateful to the Deanship of Scientific Research, King Saud University for funding through Vice Deanship of Scientific Research Chairs.

**Institutional Review Board Statement:** Not applicable.

**Informed Consent Statement:** Not applicable.

**Data Availability Statement:** Data are contained within the article.

**Acknowledgments:** We thank Tikrit and Al-Nahrain Universities for technical support.

**Conflicts of Interest:** The authors declare no conflict of interest.

## References

1. Mardani, A.; Streimikiene, D.; Cavallaro, F.; Loganathan, N.; Khoshnoudi, M. Carbon dioxide (CO<sub>2</sub>) emissions and economic growth: A systematic review of two decades of research from 1995 to 2017. *Sci. Total Environ.* **2019**, *649*, 31–49. [[CrossRef](#)] [[PubMed](#)]
2. Yaumi, A.L.; Abu Bakar, M.Z.; Hameed, B.H. Recent advances in functionalized composite solid materials for carbon dioxide capture. *Energy* **2017**, *124*, 461–480. [[CrossRef](#)]
3. Sun, H.; Xin, Q.; Ma, Z.; Lan, S. Effects of plant diversity on carbon dioxide emissions and carbon removal in laboratory-scale constructed wetland. *Environ. Sci. Pollut. Res.* **2019**, *26*, 5076–5082. [[CrossRef](#)] [[PubMed](#)]
4. Bui, M.; Adjiman, C.S.; Bardow, A.; Anthony, E.J.; Boston, A.; Brown, S.; Fennell, P.S.; Fuss, S.; Galindo, A.; Hackett, L.A.; et al. Carbon capture and storage (CCS): The way forward. *Energy Environ. Sci.* **2018**, *11*, 1062–1176. [[CrossRef](#)]
5. Intergovernmental Panel on Climate Change. Climate Change. Climate change 2007: Synthesis report. In *Contribution of Working Groups I, II and III to the Fourth Assessment Report of the Intergovernmental Panel on Climate Change*; Core Writing Team, Pachauri, R.K., Reisinger, A., Eds.; Intergovernmental Panel on Climate Change: Geneva, Switzerland, 2008; p. 104.
6. Sanz-Pérez, E.S.; Murdock, C.R.; Didas, S.A.; Jones, C.W. Direct Capture of CO<sub>2</sub> from Ambient Air. *Chem. Rev.* **2016**, *116*, 11840–11876. [[CrossRef](#)]
7. Goh, K.; Karahan, H.E.; Yang, E.; Bae, T.-H. Graphene-Based Membranes for CO<sub>2</sub>/CH<sub>4</sub> Separation: Key Challenges and Perspectives. *Appl. Sci.* **2019**, *9*, 2784. [[CrossRef](#)]
8. Jankovský, O.; Lojka, M.; Lauermannová, A.-M.; Antončík, F.; Pavlíková, M.; Pavlík, Z.; Sedmidubský, D. Carbon Dioxide Uptake by MOC-Based Materials. *Appl. Sci.* **2020**, *10*, 2254. [[CrossRef](#)]
9. Osman, A.I.; Hefny, M.; Maksoud, M.I.A.A.; Elgarahy, A.M.; Rooney, D.W. Recent advances in carbon capture storage and utilisation technologies: A review. *Environ. Chem. Lett.* **2021**. ahead of print. [[CrossRef](#)]
10. Wilberforce, T.; Olabi, A.; Sayed, E.T.; Elsaid, K.; Abdelkareem, M.A. Progress in carbon capture technologies. *Sci. Total Environ.* **2021**, *761*, 143203. [[CrossRef](#)]
11. Cannone, S.F.; Lanzini, A.; Santarelli, M. A Review on CO<sub>2</sub> Capture Technologies with Focus on CO<sub>2</sub>-Enhanced Methane Recovery from Hydrates. *Energies* **2021**, *14*, 387. [[CrossRef](#)]
12. Omodolor, I.S.; Otor, H.O.; Andonegui, J.A.; Allen, B.J.; Alba-Rubio, A.C. Dual-Function Materials for CO<sub>2</sub> Capture and Conversion: A Review. *Ind. Eng. Chem. Res.* **2020**, *59*, 17612–17631. [[CrossRef](#)]
13. Muslemanni, H.; Liang, X.; Kaesehage, K.; Wilson, J. Business Models for Carbon Capture, Utilization and Storage Technologies in the Steel Sector: A Qualitative Multi-Method Study. *Processes* **2020**, *8*, 576. [[CrossRef](#)]
14. Shukrullah, S.; Naz, M.Y.; Mohamed, N.M.; Ibrahim, K.A.; Abdel-Salam, N.M.; Ghaffar, A. CVD Synthesis, Functionalization and CO<sub>2</sub> Adsorption Attributes of Multiwalled Carbon Nanotubes. *Processes* **2019**, *7*, 634. [[CrossRef](#)]
15. Raza, A.; Gholami, R.; Rezaee, R.; Rasouli, V.; Rabiei, M. Significant aspects of carbon capture and storage—A review. *Petroleum* **2019**, *5*, 335–340. [[CrossRef](#)]
16. Li, J.; Hou, Y.; Wang, P.; Yang, B. A Review of Carbon Capture and Storage Project Investment and Operational Decision-Making Based on Bibliometrics. *Energies* **2019**, *12*, 23. [[CrossRef](#)]
17. D'Alessandro, D.M.; Smit, B.; Long, J.R. Carbon Dioxide Capture: Prospects for New Materials. *Angew. Chem. Int. Ed.* **2010**, *49*, 6058–6082. [[CrossRef](#)]

18. Shukla, S.K.; Khokarale, S.G.; Bui, T.Q.; Mikkola, J.-P.T. Ionic Liquids: Potential Materials for Carbon Dioxide Capture and Utilization. *Front. Mater.* **2019**, *6*, 42. [\[CrossRef\]](#)
19. Mukherjee, A.; Okolie, J.A.; Abdelrasoul, A.; Niu, C.; Dalai, A.K. Review of post-combustion carbon dioxide capture technologies using activated carbon. *J. Environ. Sci.* **2019**, *83*, 46–63. [\[CrossRef\]](#)
20. Okesola, A.A.; Oyedeji, A.A.; Abdulhamid, A.F.; Olowo, J.; Ayodele, B.E.; Alabi, T.W. Direct Air Capture: A Review of Carbon Dioxide Capture from the Air. *IOP Conf. Ser. Mater. Sci. Eng.* **2018**, *413*, 012077. [\[CrossRef\]](#)
21. Luis, P. Use of monoethanolamine (MEA) for CO<sub>2</sub> capture in a global scenario: Consequences and alternatives. *Desalination* **2016**, *380*, 93–99. [\[CrossRef\]](#)
22. Rochelle, G.T. Amine scrubbing for CO<sub>2</sub> capture. *Science* **2009**, *325*, 1652–1654. [\[CrossRef\]](#) [\[PubMed\]](#)
23. Electric Power Research Institute. *Program on Technology Innovation: Post-Combustion CO<sub>2</sub> Capture Technology Development*; Electric Power Research Institute: Palo Alto, CA, USA, 2008.
24. Figueroa, J.D.; Fout, T.; Plasynski, S.; McIlvried, H.; Srivastava, R.D. Advances in CO<sub>2</sub> capture technology—The U.S. Department of Energy’s Carbon Sequestration Program: A review. *Int. J. Greenh. Gas Control* **2008**, *2*, 9–20. [\[CrossRef\]](#)
25. Asadi-Sangachini, Z.; Galangash, M.M.; Younesi, H.; Nowrouzi, M. The feasibility of cost-effective manufacturing activated carbon derived from walnut shells for large-scale CO<sub>2</sub> capture. *Environ. Sci. Pollut. Res.* **2019**, *26*, 26542–26552. [\[CrossRef\]](#) [\[PubMed\]](#)
26. Gibson, J.A.A.; Mangano, E.; Shiko, E.; Greenaway, A.G.; Gromov, A.V.; Lozinska, M.M.; Friedrich, D.; Campbell, E.E.B.; Wright, P.A.; Brandani, S. Adsorption Materials and Processes for Carbon Capture from Gas-Fired Power Plants: AMPGas. *Ind. Eng. Chem. Res.* **2016**, *55*, 3840–3851. [\[CrossRef\]](#)
27. Lee, S.-Y.; Park, S.-J. A review on solid adsorbents for carbon dioxide capture. *J. Ind. Eng. Chem.* **2015**, *23*, 1–11. [\[CrossRef\]](#)
28. Lee, S.C.; Chae, H.J.; Lee, S.J.; Choi, B.Y.; Yi, C.K.; Lee, J.B.; Ryu, C.K.; Kim, J.C. Development of Regenerable MgO-Based Sorbent Promoted with K<sub>2</sub>CO<sub>3</sub> for CO<sub>2</sub> Capture at Low Temperatures. *Environ. Sci. Technol.* **2008**, *42*, 2736–2741. [\[CrossRef\]](#)
29. Wang, S.; Yan, S.; Ma, X.; Gong, J. Recent advances in capture of carbon dioxide using alkali-metal-based oxides. *Energy Environ. Sci.* **2011**, *4*, 3805–3819. [\[CrossRef\]](#)
30. Hauchhum, L.; Mahanta, P. Carbon dioxide adsorption on zeolites and activated carbon by pressure swing adsorption in a fixed bed. *Int. J. Energy Environ. Eng.* **2014**, *5*, 349–356. [\[CrossRef\]](#)
31. Staciwa, P.; Narkiewicz, U.; Sibera, D.; Moszyński, D.; Wróbel, R.J.; Cormia, R.D. Carbon Spheres as CO<sub>2</sub> Sorbents. *Appl. Sci.* **2019**, *9*, 3349. [\[CrossRef\]](#)
32. Aquino, A.S.; Vieira, M.O.; Ferreira, A.S.D.; Cabrita, E.J.; Einloft, S.; De Souza, M.O. Hybrid Ionic Liquid–Silica Xerogels Applied in CO<sub>2</sub> Capture. *Appl. Sci.* **2019**, *9*, 2614. [\[CrossRef\]](#)
33. Chiang, Y.-C.; Yeh, C.-Y.; Weng, C.-H. Carbon Dioxide Adsorption on Porous and Functionalized Activated Carbon Fibers. *Appl. Sci.* **2019**, *9*, 1977. [\[CrossRef\]](#)
34. Choma, J.; Kloske, M.; Dziura, A.; Stachurska, K.; Jaroniec, M. Preparation and Studies of Adsorption Properties of Microporous Carbon Spheres. *Eng. Prot. Environ.* **2016**, *19*, 169–182. [\[CrossRef\]](#)
35. Dawson, R.; Cooper, A.I.; Adams, D.J. Nanoporous organic polymer networks. *Prog. Polym. Sci.* **2012**, *37*, 530–563. [\[CrossRef\]](#)
36. Choi, S.; Drese, J.H.; Jones, C.W. Adsorbent Materials for Carbon Dioxide Capture from Large Anthropogenic Point Sources. *ChemSusChem* **2009**, *2*, 796–854. [\[CrossRef\]](#)
37. Wang, W.; Zhou, M.; Yuan, D. Carbon dioxide capture in amorphous porous organic polymers. *J. Mater. Chem. A* **2017**, *5*, 1334–1347. [\[CrossRef\]](#)
38. Ahmed, D.S.; El-Hiti, G.A.; Yousif, E.; Ali, A.A.; Hameed, A.S. Design and synthesis of porous polymeric materials and their applications in gas capture and storage: A review. *J. Polym. Res.* **2018**, *25*, 75. [\[CrossRef\]](#)
39. Spadaro, L.; Arena, F.; Negro, P.; Palella, A. Sunfuels from CO<sub>2</sub> exhaust emissions: Insights into the role of photoreactor configuration by the study in laboratory and industrial environment. *J. CO<sub>2</sub> Util.* **2018**, *26*, 445–453. [\[CrossRef\]](#)
40. Ouyang, Y.; Yang, H.; Zhang, P.; Wang, Y.; Kaur, S.; Zhu, X.; Wang, Z.; Sun, Y.; Hong, W.; Ngeow, Y.F.; et al. Synthesis of 2,4-Diaminopyrimidine Core-Based Derivatives and Biological Evaluation of Their Anti-Tubercular Activities. *Molecules* **2017**, *22*, 1592. [\[CrossRef\]](#)
41. Masur, H.; Brooks, J.T.; Benson, C.A.; Holmes, K.K.; Pau, A.K.; Kaplan, J.E. Prevention and Treatment of Opportunistic Infections in HIV-Infected Adults and Adolescents: Updated Guidelines From the Centers for Disease Control and Prevention, National Institutes of Health, and HIV Medicine Association of the Infectious Diseases Society of America. *Clin. Infect. Dis.* **2014**, *58*, 1308–1311. [\[CrossRef\]](#)
42. Mousa, O.G.; Yousif, E.; Ahmed, A.A.; El-Hiti, G.A.; Alotaibi, M.H.; Ahmed, D.S. Synthesis and use of carvedilol metal complexes as carbon dioxide storage media. *Appl. Petrochem. Res.* **2020**, *10*, 157–164. [\[CrossRef\]](#)
43. Hadi, A.G.; Jawad, K.; Yousif, E.; El-Hiti, G.A.; Alotaibi, M.H.; Ahmed, D.S. Synthesis of Telmisartan Organotin(IV) Complexes and their use as Carbon Dioxide Capture Media. *Molecules* **2019**, *24*, 1631. [\[CrossRef\]](#) [\[PubMed\]](#)
44. Mohammed, A.; Yousif, E.; El-Hiti, G.A. Synthesis and Use of Valsartan Metal Complexes as Media for Carbon Dioxide Storage. *Materials* **2020**, *13*, 1183. [\[CrossRef\]](#) [\[PubMed\]](#)
45. Mahmood, Z.N.; Alias, M.; El-Hiti, G.A.-R.; Ahmed, D.S.; Yousif, E. Synthesis and use of new porous metal complexes containing a fusidate moiety as gas storage media. *Korean J. Chem. Eng.* **2021**, *38*, 179–186. [\[CrossRef\]](#)

46. Omer, R.M.; Al-Tikrity, E.T.B.; El-Hiti, G.A.; Alotibi, M.F.; Ahmed, D.S.; Yousif, E. Porous Aromatic Melamine Schiff Bases as Highly Efficient Media for Carbon Dioxide Storage. *Processes* **2020**, *8*, 17. [[CrossRef](#)]
47. Mohamed, S.H.; Hameed, A.S.; Yousif, E.; Alotaibi, M.H.; Ahmed, D.S.; El-Hiti, G.A. New Porous Silicon-Containing Organic Polymers: Synthesis and Carbon Dioxide Uptake. *Processes* **2020**, *8*, 1488. [[CrossRef](#)]
48. Ahmed, D.S.; El-Hiti, G.A.; Yousif, E.; Hameed, A.S.; Abdalla, M. New Eco-Friendly Phosphorus Organic Polymers as Gas Storage Media. *Polymers* **2017**, *9*, 336. [[CrossRef](#)]
49. Satar, H.A.; Ahmed, A.A.; Yousif, E.; Ahmed, D.S.; Alotibi, M.F.; El-Hiti, G.A. Synthesis of Novel Heteroatom-Doped Porous-Organic Polymers as Environmentally Efficient Media for Carbon Dioxide Storage. *Appl. Sci.* **2019**, *9*, 4314. [[CrossRef](#)]
50. Donald, A.M. The use of environmental scanning electron microscopy for imaging wet and insulating materials. *Nat. Mater.* **2003**, *2*, 511–516. [[CrossRef](#)]
51. Thommes, M.; Kaneko, K.; Neimark, A.V.; Olivier, J.P.; Rodriguez-Reinoso, F.; Rouquerol, J.; Sing, K.S. Physisorption of gases, with special reference to the evaluation of surface area and pore size distribution (IUPAC Technical Report). *Pure Appl. Chem.* **2015**, *87*, 1051–1069. [[CrossRef](#)]
52. Sotomayor, F.J.; Cychosz, K.A.; Thommes, M. Characterization of micro/mesoporous materials by physisorption: Concepts and case studies. *Acc. Mater. Surf. Res.* **2018**, *3*, 34–50.
53. Sing, K. The use of nitrogen adsorption for the characterisation of porous materials. *Colloids Surfaces A Physicochem. Eng. Asp.* **2001**, *187–188*, 3–9. [[CrossRef](#)]
54. Cychosz, K.A.; Thommes, M. Progress in the Physisorption Characterization of Nanoporous Gas Storage Materials. *Engineering* **2018**, *4*, 559–566. [[CrossRef](#)]
55. Arena, F.; Trunfio, G.; Negro, J.; Spadaro, L. Optimization of the MnCeO<sub>x</sub> system for the catalytic wet oxidation of phenol with oxygen (CWAO). *Appl. Catal. B Environ.* **2008**, *85*, 40–47. [[CrossRef](#)]
56. Bonenfant, D.; Kharoune, M.; Niquette, P.; Mimeault, M.; Hausler, R. Advances in principal factors influencing carbon dioxide adsorption on zeolites. *Sci. Technol. Adv. Mater.* **2008**, *9*, 013007. [[CrossRef](#)]
57. Kim, K.C.; Jang, S.S. Molecular Simulation Study on Factors Affecting Carbon Dioxide Adsorption on Amorphous Silica Surfaces. *J. Phys. Chem. C* **2020**, *124*, 12580–12588. [[CrossRef](#)]